Supporting Information

Dual Promotion of Oxygen Reduction on Pt in Membrane Electrode Assembly by Hydroxyphenyl Metal Porphyrins

Meihua Tang,[a†] Chunping Wang,[a†] Zhenying Zheng,[a] Xiaoxiao Wang,[a] Fulong Zhu[a] and Shengli Chen[*a]

a Hubei Key Laboratory of Electrochemical Power Sources, College of Chemistry and Molecular Sciences, Wuhan University, Wuhan 430072, P. R. China

* Corresponding author: slchen@whu.edu.cn

† These authors contributed equally to this work

1. Experimental section

1.1 Materials

40 wt% Pt/C catalyst (Johnson Matthey), 5 wt% Nafion solution (DuPont D520), isopropanol (99.5%+, Aladdin), Nafion membrane (NRE 211, 25μm, DuPont), gas diffusion layers (GDLs, TGP-H-060, Toray), meso-5,10,15,20-tetra (4-hydroxyphenyl) porphyrin (POH, 95%+, Aladdin), meso-5,10,15,20-tetra (4-sulfonicphenyl) cobalt porphyrin (PSO_3H, 95%+, Aladdin), Dimethylformamide (DMF) (Sinopbarm Chemical Reagent Co., Ltd), cobalt acetate ($(CH_3COO)_2Co{\cdot}4H_2O$), nickel acetate ($(CH_3COO)_2Ni{\cdot}4H_2O$), copper acetate ($(CH_3COO)_2Cu{\cdot}4H_2O$), zinc acetate ($(CH_3COO)_2Zn{\cdot}4H_2O$) (Sinopbarm Chemical Reagent Co.,Ltd 99.5%+). All materials were used as received.

1.2 Synthesis of hydroxyphenyl metal porphyrins (MPOHs)

MPOH was synthesized according to the literature[1]. As shown in Fig. S1, 0.1 g POH and 0.35 g $(CH_3COO)_2M{\cdot}4H_2O$ were ground in an agate mortar for 30 min, followed by a dissolution in 30 mL DMF. Subsequently, the mixture was heated to 85 ℃ and the reaction lasted for 2 h while refluxing. When the reaction was completed and cooled down to room temperature, the resulting solution was poured into ice water to precipitating 12 h. The precipitates were then dispersed in deionized (DI) water and centrifuged at 10000 rpm for 8 min, and the whole process was repeated three times. Finally, the obtained solid was washed using DI water thoroughly and dried at 80 ˚C overnight to obtain the MPOH products.

The resulted products were firstly characterized by Fourier transform infrared (FTIR) absorption spectroscopy, which were recorded at the range of 250~4250 cm^{-1} under ambient conditions (ReactIR^{TM} 4000 spectrometer). Each sample was mixed and ground with KBr at a sample/KBr mass ratio of 1/200 before testing. As shown in Fig. S2, the N-H stretching vibration peak at 967 cm^{-1} disappeared and a strong N-M characteristic peak at ~1000 cm^{-1} emerged, indicating successful metalation of POH.[2] Additionally, an Ultraviolet-visible (UV-VIS) spectrophotometer (Shimadzu UV-2500) was used to the obtain the UV-VIS spectra of the free POH ligand and MPOH

dispersed in an IPA/water solution system. As shown in Fig. S3, it can be observed that there was a transformation of the four Q-bands, ranging from 500 to 660 nm, into a single band at 500 nm, which was due to the increased symmetry following the coordination of metal ions to the POH molecules.[3] These spectral results confirmed the successful synthesis of the expected MPOH compounds.

For comparison, the meso-5,10,15,20-tetra(4-sulfonicphenyl) cobalt porphyrin (denoted as $CoPSO_3H$) was also prepared using the same method, but only changed the POH reactant to PSO_3H.

1.3 MEAs preparation

Firstly, the MPOH-Nafion dispersions were prepared by dispersing a certain amount of MPOH in 5wt% Nafion solution. The cathodic ink was then prepared by mixing Pt/C catalysts, MPOH-Nafion ionomer, isopropanol (IPA)/water mixture, achieving a Nafion/carbon (N/C) mass ratio of 0.5 and a final solid concentration of 3 mg mL^{-1}. By employing gas-assisted spraying method, the CLs were directly deposited onto two sides of a Nafion 211 membrane to form the catalyst coated membrane (CCM). Each CCM had an active area of 4 cm^2 (2 cm×2 cm). Assembling the CCM with GDLs give the MEA, denoted as MPOH-Nafion-Pt/C. A conventional MEA without MPOH addition in cathodic CL (CCL) was also prepared by the same way and quoted as Nafion-Pt/C. In all MEAs, both the anode CLs and CCLs possessed a Pt loading of 0.1 mg cm^{-2}.

1.4 Physical characterization

X-ray photoelectron spectroscopy (XPS) was performed under ultrahigh vacuum at room temperature using an ESCALAB Xi^+ spectrometer (Thermo Fisher Scientific). All binding energies were referred to the binding energy of 284.8 eV from C 1s peak. The aforementioned CCL ink was sprayed on the one side of PEM and subsequently dried at 80 ˚C for 1h to obtain the tested samples.

Field-emission scanning electron microscope (FESEM) was performed on a Zeiss Merlin Compact operating at an accelerating voltage of 5 kV to characterize the

microscopic morphologies of CCL.

Dynamic light scattering (DLS) measurements were conducted using a Zetasizer ZEN 3600 instrument to analyze the aggregate size of the catalyst ink. Before testing, the cathodic ink was diluted 100 times by IPA to avoid multiple scattering.

The ionic domain sizes of Nafion with/without MPOH addition were characterized by high-resolution transmission electron microscopy (TEM) using JEM-2100 Plus instrument with an accelerating voltage of 200 kV. For sample preparation, diluted ionomer solutions with/without CoPOH were firstly drop-coated onto ultrathin carbon films and dried under an infrared lamp, followed by immersion in 0.5 M lead acetate solution for 12 hours. Then, the stained samples were rinsed with DI water and dried under vacuum at 80 ˚C for 2 hours.

1.5 Electrochemical characterization

Rotating disk electrode (RDE) testing were carried out with an electrochemical workstation (CHI 660E) connected in a three-electrode configuration at room temperature using a Pt foil and saturated calomel electrode (SCE) as the counter electrode and reference electrode, respectively. To prepare the working electrode, catalyst ink with N/C ratio of 0.5 was drop-casted on glassy carbon electrodes with a diameter of 5 mm, achieving a desired Pt loading of 60 μg cm^{-2}. The ORR activity was measured in 0.1 M $HClO_4$ saturated with O_2 at 1600 r.p.m using positive-going linear sweep voltammetry (LSV) at a scan rate of 5 mV s^{-1}.

Fuel cell testing was carried out in a fuel cell test station (Scribner 850e) using a single cell with a 5 cm^2 serpentine flow channel. The cell temperature was set to be 80 ˚C and the relative humidity (RH) was 100%. In H_2-O_2 cells, the gas flow rates were constant at 0.6 L min^{-1} under ambient conditions for both electrodes. In H_2-air cells, both the back pressure is 150 kPa and the gas flow rates for H_2 and air were constant at 0.3 L min^{-1} and 0.5 L min^{-1}, respectively. The test protocol involved in a linear current mode with a recording step of 1 min per point. In H_2-air cells, electrochemical impedance spectroscopy (EIS) measurements at constant current densities were also conducted by using the equipped frequency analyzer (885) from 10 kHz to 0.1 Hz.

The evaluation of sulfonate coverage was obtained via CO displacement and stripping experiments with a potentiostat (CorrTest CS2350M). The experiments were conducted at 60 ˚C with 1 atm 5% H_2-N_2 and pure N_2 or 1% CO-N_2 flowing at 0.6 L min^{-1} feeding for anode and cathode lines, respectively. The test of CO displacement involved measuring the transient current response (*I-t*) resulting from the introduction of CO to the equilibrated MEA held at 0.4 V. After purging CO for 5 min, the cathodic gas was then switched to pure N_2, and CO stripping test was performed by sweeping the cell voltage from 0.1 to 1.23 V at a scan rate of 20 mV s^{-1}.

Limiting current (i_{lim}) measurements at 80 ˚C and 100% RH were performed to evaluate the oxygen transport resistance, with 0.3 L min^{-1} of H_2 and 0.3 mL min^{-1} O_2-N_2 mixing gas (x_{O2} = 1, 2, 3, and 4%.) purging into the anode and cathode, respectively. LSVs were conducted from the open circuit voltage (OCV) to 0.15 V with a scan rate of 5 mV s^{-1}, where the maximum current density above 0.12 V was determined as the i_{lim}.

The proton transport resistance (R_{H+}) in CCL was measured by EIS method at 80˚C and 100%RH using a potentiostat (BioLogic SP300). 1 atm pure H_2 and N_2 were supplied at the anode and cathode at flow rates of 0.2 L min^{-1}, respectively. The EIS analysis was performed at 0.4 V, with 15 mV AC amplitude from 100 kHz to 100 mHz.

The electrochemical surface area (ECSA) was calculated from the integral charges corresponding to the hydrogen desorption peak (0.1~0.4 V) in cyclic voltammetry (CV) obtained in a potential range of 0.1 V to 1.23 V at a scan rate of 500 mV s^{-1} using a potentiostat (CorrTest CS2350M). The feeding gas conditions are the same as that used for measuring the R_{H+}.

1.6 Molecular dynamics (MD) simulations

1.6.1 Simulation parameters. The force fields of Nafion and Pt were taken from the work of Mabuchi et al.[4] and He et al.[5], respectively. And the classical hydronium models[6] and f3C models[7] were applied for hydronium ions and water molecules, respectively. For CoPOH and isopropanol (IPA) molecules, CHARMM force field[8] were employed. The Lorentz-Bertelot mixing rule was used for analyzing the

interaction between different atoms, with a cutoff distance of 1.5 nm. Long-range electrostatic interactions were calculated using the particle-mesh Ewald method with an accuracy of 0.0001. The temperature was controlled by the Nose-Hoover thermostat, and the isotropic pressure was kept by the Parrinello-Rahman method. And the time step for the simulations was set to 1.0 fs. All simulations were performed using the Large-scale Atomic/Molecular Massively Parrel Simulator (LAMMPS) package.[9]

1.6.2 Simulation of CLs. The structures of the Nafion and CoPOH used in the simulations are shown in Fig. S7. The simulation model contains of eight layers of Pt (100) with a layered distance of 1.96 Å, where the box sizes are set as 7.76 nm in the X and Y directions, and the Pt layers are considered to be fixed during the simulations. The Nafion polymer chains possess 13 sulfonates and 13 hydronium ions, and have an equivalent weight (EW) of 1100, which is similar to that generally used in experiments. Firstly, 10 Nafion chains, 130 hydronium ions, 945 IPA molecules, 875 water molecules, and CoPOH molecules were randomly placed on the Pt layers. Periodic boundary conditions (PBC) are used in the X-Y direction, and Z-direction is set at a height of 30 nm. Then, repeated annealing processes of solvent removal followed by re-equilibration of the remaining system are conducted for five times to obtain the equilibrated ionomer film covering the Pt surface, including a) NVT simulation for 3 ns at 1000 K using the LJ parameter (ε) within Nafion atoms reduced by two orders of magnitude; b) NVT simulation for 3 ns returning the LJ parameter (ε) to the original value and the temperature to 353 K. In addition, the fixed wall 10 ns from the catalyst support during the simulation was set to prevent dispersion solvent from escaping. Subsequently, NVT simulations for 10 ns at 353 K were performed for product progress, in which the fixed wall was set high enough (30 nm from catalyst support) to avoid interaction, and the potential of the fixed wall was set as follows:

$$E_{wall} = \begin{cases} 4\varepsilon_{wall}\left[\left(\frac{\sigma_{wall}}{r_{wall}}\right)^{12} - \left(\frac{\sigma_{wall}}{r_{wall}}\right)^{6}\right] r_{wall} \leq 0.25\ nm \\ 0 \quad r_{wall} > 0.25nm \end{cases}$$

where r_{wall} is the distance between the wall and atoms. The parameters σ_{wall} and ε_{wall} are set as 0.01 kcal mol^{-1} and 0.25 nm, respectively. Finally, the Nafion film

system with solvent molecules was obtained.

The hydrated oxygen transport process was simulated by inserting oxygen and water molecules into the gas region at the top of PFSA equilibrium film. It is worth noting that only several O_2 molecules exist under the pressure of 1atm due to the nanoscale box, which leads to a large error due to few samples. Consequently, the number of oxygen molecules was set as 750, which corresponded to the pressure of ~25 MPa for ensuring sufficient statistical sampling to improve the reliability and accuracy of the simulation results. This should not affect the local oxygen transport resistances since they are pressure-independent. When an oxygen molecule reaches a region within 0.31 nm from the Pt surface, it will be removed from the simulation box, and a new oxygen molecule will be added at the top of the gas region to maintain a constant number of oxygen molecules. For each condition, a 20 ns MD simulation was executed to calculated the oxygen permeation flux J_{Pt} (mol s^{-1} m^{-2}) by

$$J_{Pt} = \frac{N_O}{N_A A \Delta t}$$

where N_O is the number of oxygen molecules that reached the surface of Pt, N_A is the Avogadro constant, A is the surface area, and Δt is the diffusion time, and the oxygen transport resistance R (A^{-1} m^2 Pa) was calculated by:

$$R = \frac{\Delta P}{4 F J_{Pt}}$$

where ΔP represents the oxygen pressure difference between the gas region and the Pt surface, and F is the Faraday constant. The number of oxygen molecules in Pt surface is 0, and thus the pressure is 0.

1.7 Density Functional Theory (DFT) calculations

The spin-polarized calculations under DFT were performed using the Vienna *ab initio* simulation package (VASP).[10] The Perdew–Burke–Ernzerhof (PBE) functional within generalized gradient approximation (GGA)[11] was employed to describe the electron exchange-correlation interactions. The structure of a porphyrin and the adsorbed oxygen molecule contained 83 atoms and had a size of 13 Å × 13 Å × 4 Å. It

was placed in a cubic supercell with lattice parameters of 25 Å × 25 Å × 20 Å to minimize the interactions between neighboring images. The plane-wave energy cut-off was set as 450 eV for the expansion of electronic wave function, and a Gaussian smearing method with an energy broadening of 0.05 eV were used. Only Γ-point was adopted for sampling the Brillouin zone. All the geometries were fully optimized until the maximal components of force on each atom were converged to less than 10^{-2} eV $Å^{-1}$.

For the chemisorption step of O_2 molecule, the free energy change is calculated by the following equation:

$$\Delta G = \Delta E + \Delta ZPE - T\Delta S \quad (1)$$

where ΔE is the total energy difference between the reactant and product during the chemisorption processes, and ΔZPE are $T\Delta S$ the changes in the zero-point energy and the entropic contribution, respectively.[12]

2. SI Figures

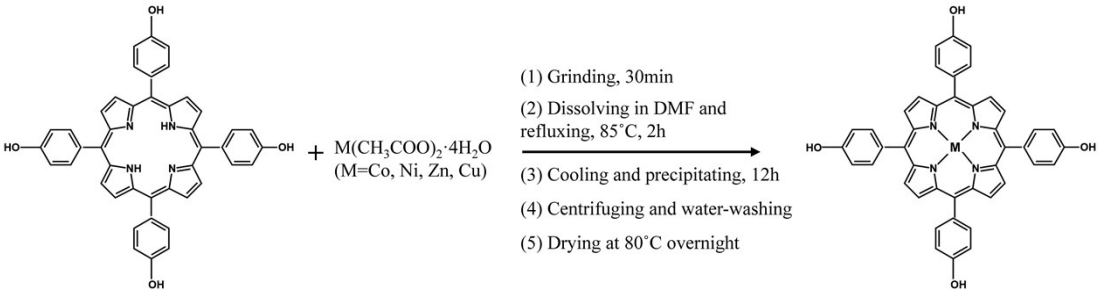

Fig. S1 Synthesis procedure of MPOH (M=Co, Ni, Zn, Cu).

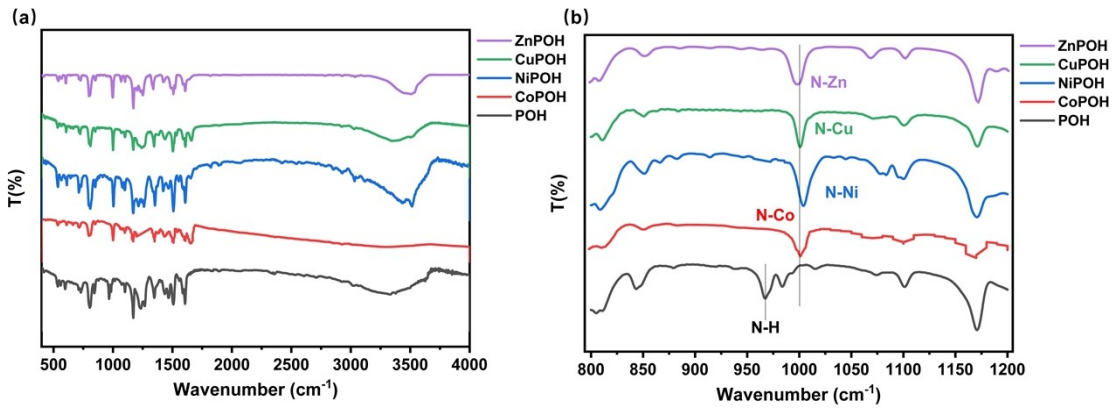

Fig. S2 (a) FTIR spectra of POH and MPOH; (b) the FTIR spectra with wavenumber ranging from 800 cm^{-1} to 1200 cm^{-1}, where the characteristic peak of N-H and N-M locating at 967 cm^{-1} and 1000 cm^{-1}, respectively.

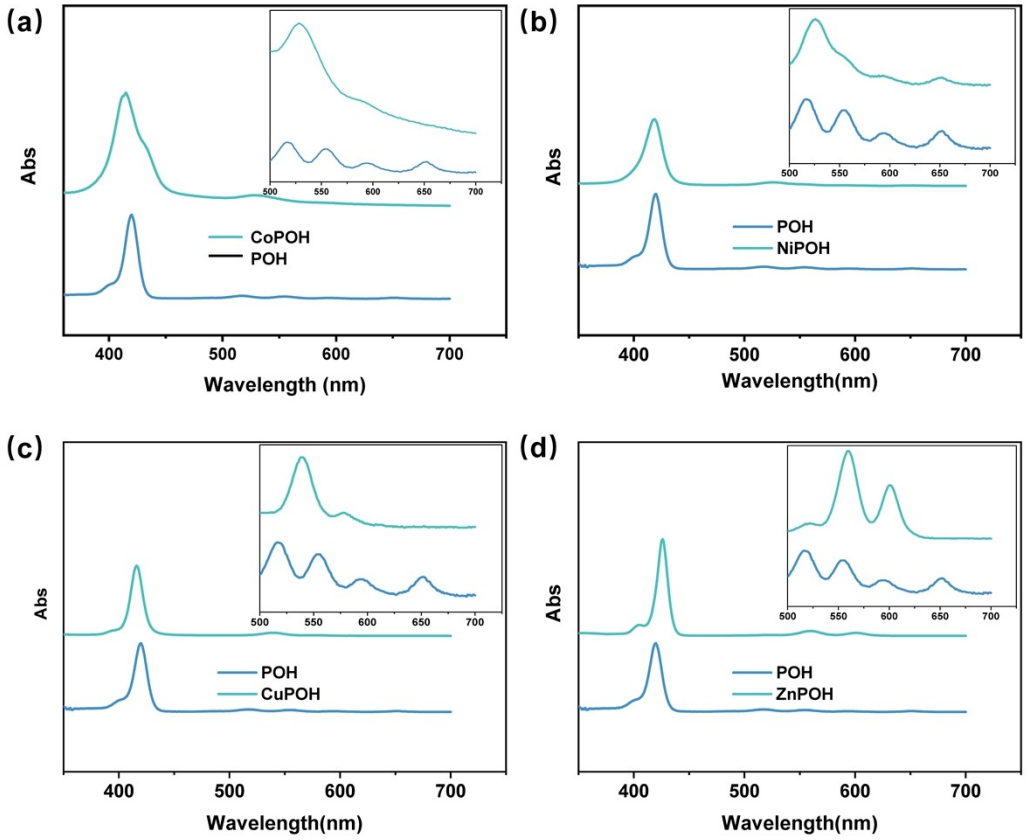

Fig. S3 UV-Visible spectra of POH and (a) CoPOH (b) NiPOH (c) CuPOH (d) ZnPOH. The insets in figures represent the UV-Visible spectra with wavelength ranging from 500 nm to 700 nm.

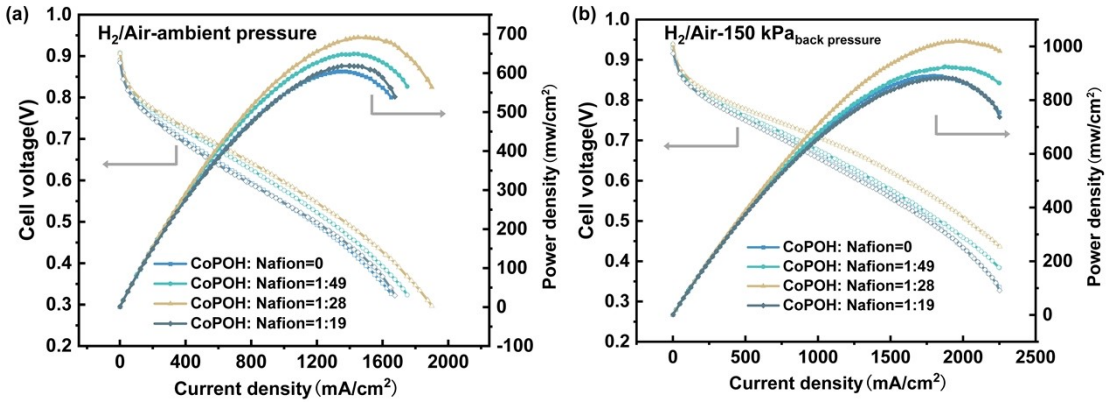

Fig. S4 H_2-air fuel cell polarization curves (without *iR* correction) and power density plots of the cells with different mass ratios between CoPOH and Nafion under (a) ambient pressure (b) 150 $kPa_{back\ pressure}$. All the single cells are measured at 80 ˚C, 100%RH; and the flow rates of H_2 and air were 0.3 L min^{-1} and 0.5 L min^{-1}, respectively.

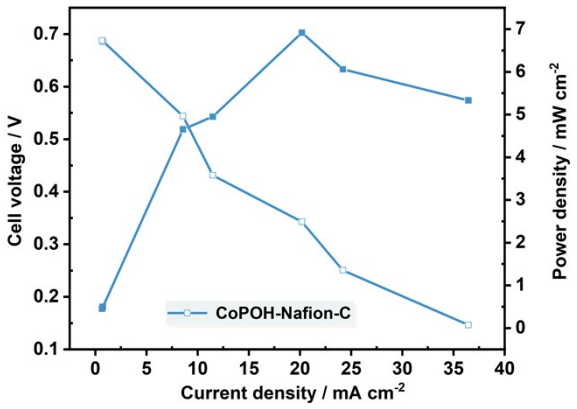

Fig. S5 Polarization curves (without *iR* correction) and power density plots of fully humidified H_2-O_2 cell with MEA of CoPOH-Nafion-C. The cell was tested at 80 ˚C, ambient pressure. The flow rates of H_2 and O_2 were both constant at 600 mL min^{-1}.

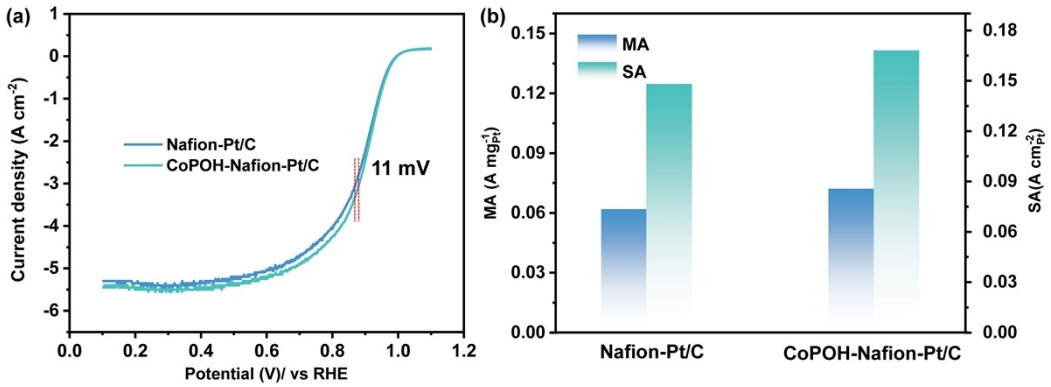

Fig. S6 (a) LSV curves and (b) calculated mass activity (MA) and specific activity (SA) at 0.9 V of Pt/C catalysts with Nafion and CoPOH-Nafion as the binder in the RDE measurements.

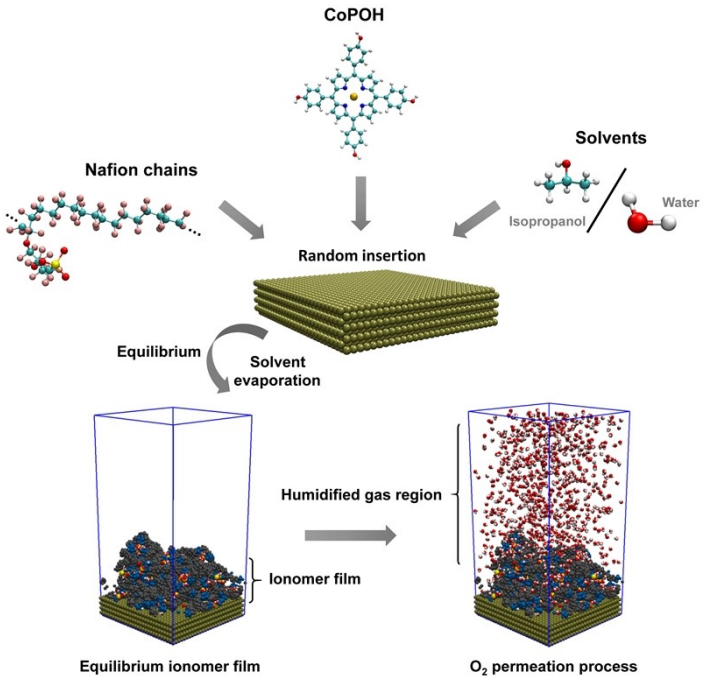

Fig. S7 Structures, equilibrium process and oxygen permeation process during the MD simulation.

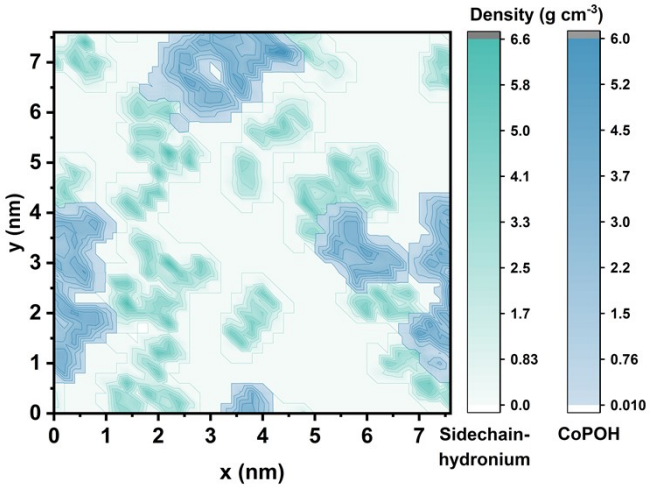

Fig. S8 Density distribution of Nafion's side chain-hydronium regions and CoPOH within the Pt/ionomer interface region.

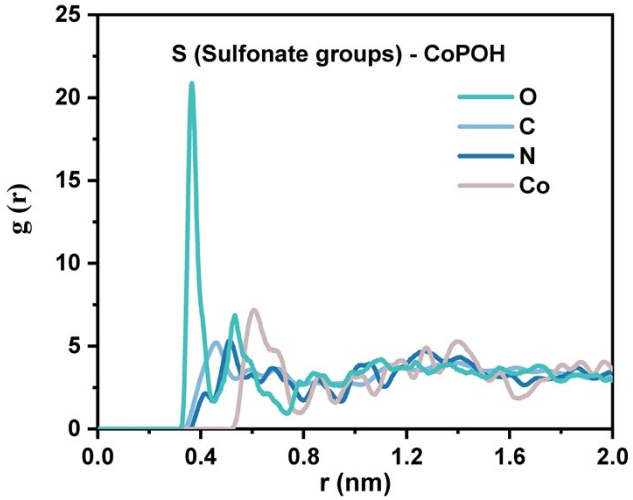

Fig. S9 Radial distribution functions (RDFs) between S atom in $-SO_3^-$ of Nafion and atoms in CoPOH.

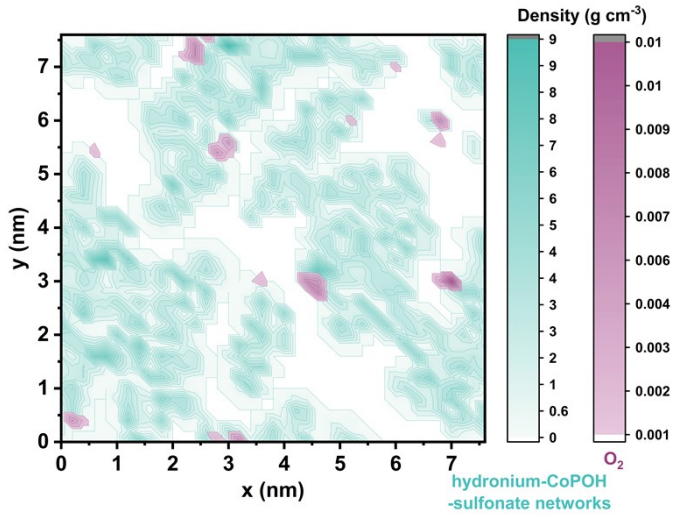

Fig. S10 Density distribution of oxygen and Nafion side chains-hydronium-CoPOH networks within the Pt/ionomer interface region.

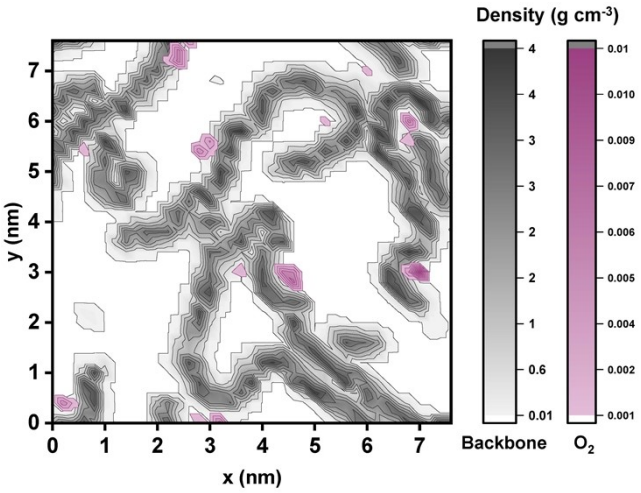

Fig. S11 Density distribution of Nafion's backbones and oxygen within the Pt/ionomer interface region.

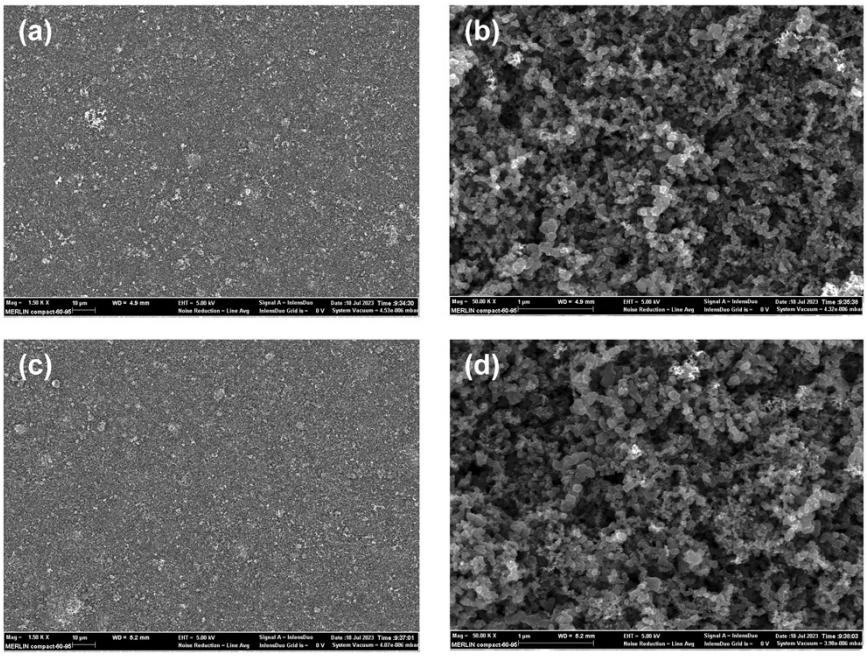

Fig. S12 SEM images of CCLs: (a, b) Nafion-Pt/C; (c.d) CoPOH-Nafion-Pt/C.

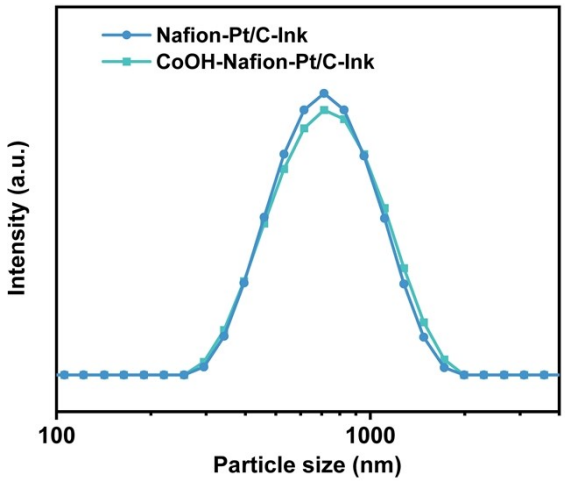

Fig. S13 Particle size distribution curves of catalyst inks for Nafion-Pt/C and CoPOH-Nafion-Pt/C.

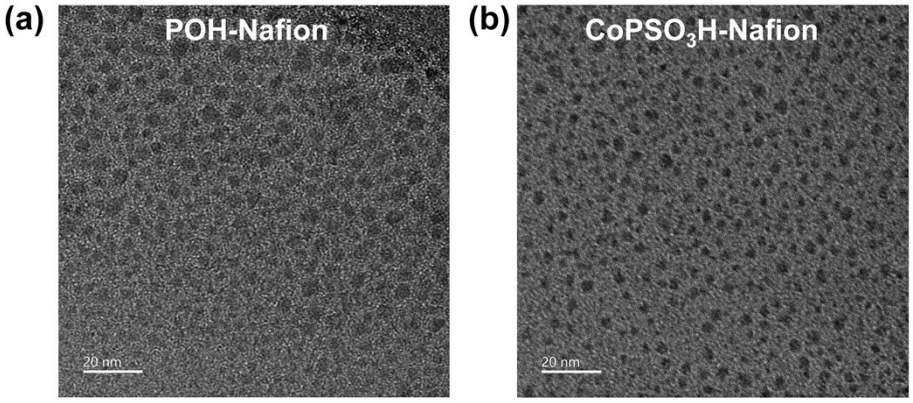

Fig. S14 High-resolution TEM images of films casting by Pb^{2+}-staining solution of (a) POH-Nafion and (b) $CoPSO_3H$-Nafion. The dark areas indicate the ionic domains.

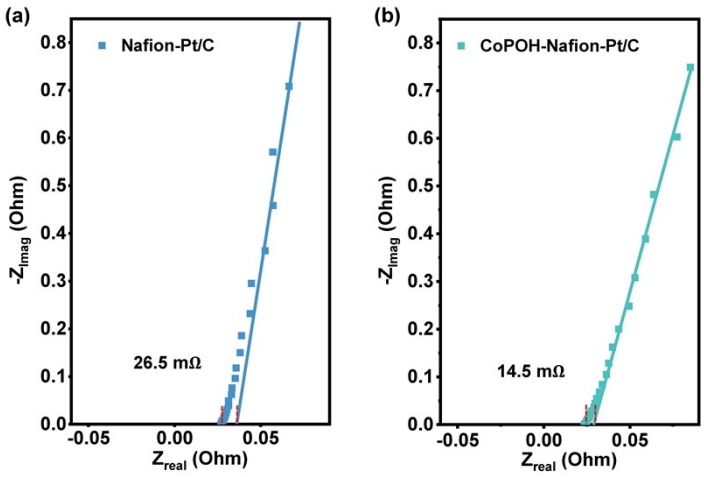

Fig. S15 Nyquist plots of EIS spectra and the estimated proton transport resistance (R_{H+}) at 0.4 V under H_2/N_2: (a) Nafion-Pt/C and (b) CoPOH-Nafion-Pt/C.

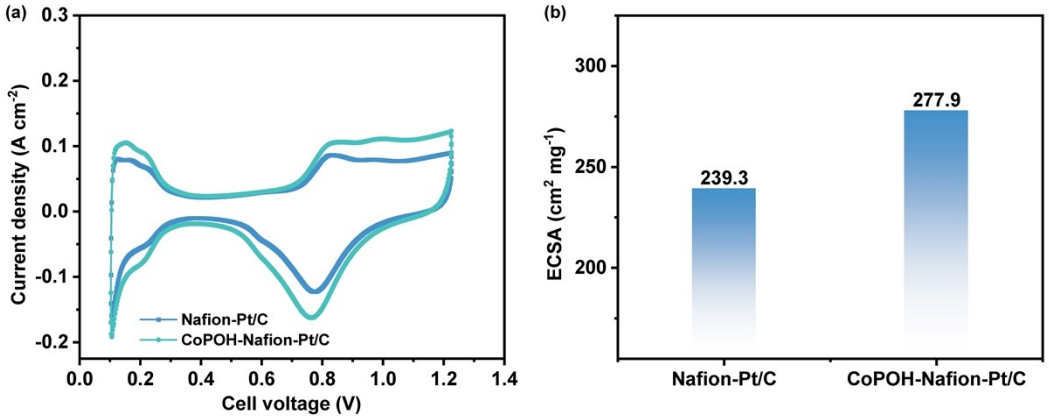

Fig. S16 (a) CV curves and (b) the calculated ECSA values according to the hydrogen desorption charge in CV.

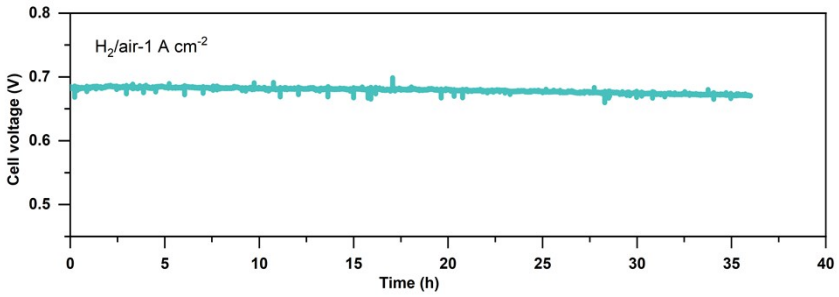

Fig. S17 Stability test of the cell with CoPOH-Nafion-Pt/C in H_2-air fuel cell at an output current density of 1 A cm^{-2}.

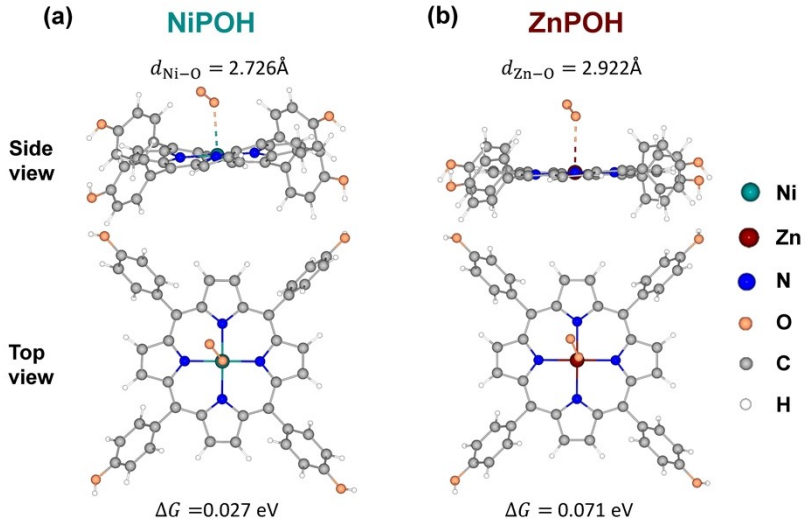

Fig. S18 Equilibrium structures of the system after oxygen adsorption by (a) NiPOH (b) ZnPOH based on DFT calculations.

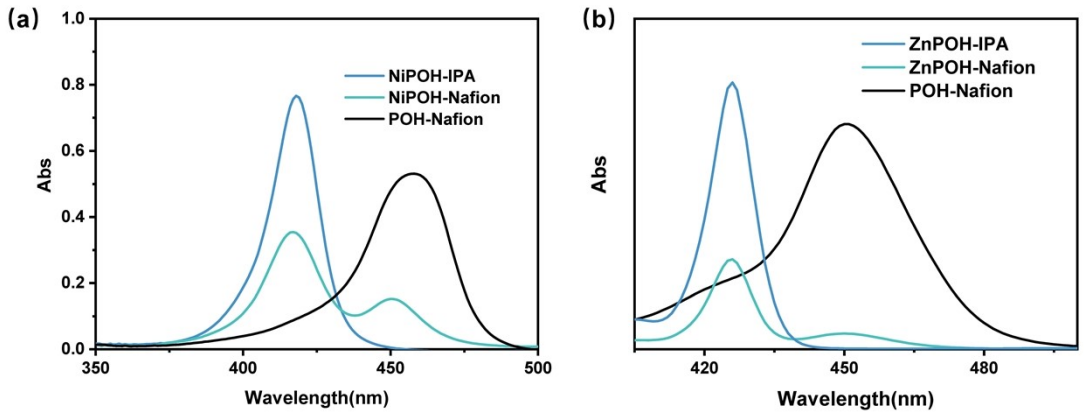

Fig. S19 UV-Vis spectra of (a) NiPOH-Nafion mixture and (b) NiPOH-Nafion mixture. For comparison, the spectra of NiPOH-isopropanol dispersion, ZnPOH-isopropanol dispersion and POH-Nafion are also shown in the figures.

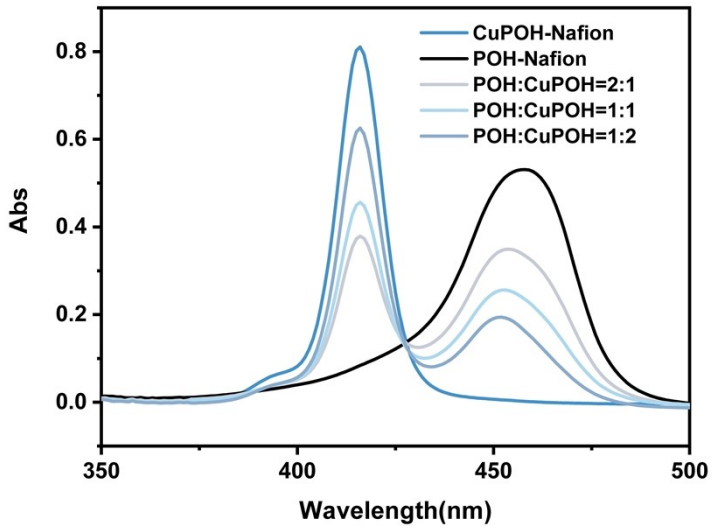

Fig. S20 UV-Vis spectra of CuPOH-Nafion mixture and CuPOH-POH-Nafion mixtures with with different POH to CoPOH mass ratios (2:1, 1:1, 1:2). For comparison, the spectra of POH-Nafion is also shown in the figure.

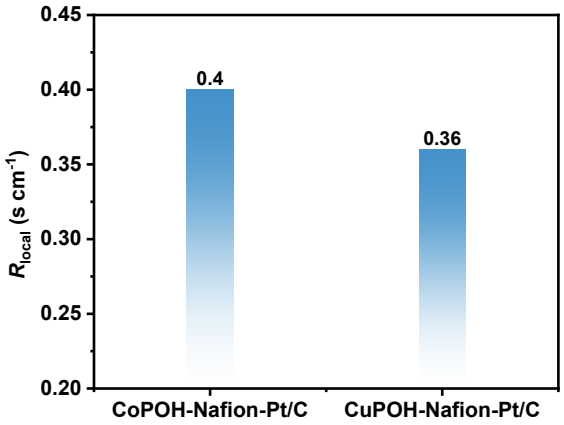

Fig. S21 Comparison of R_{local} between CoPOH-Nafion-Pt/C and CuPOH-Nafion-Pt/C.

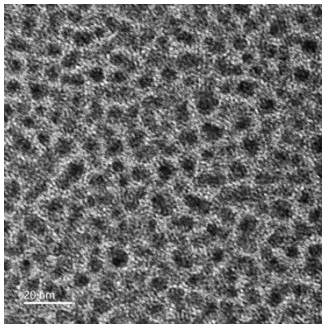

Fig. S22 High-resolution TEM images of films casting by Pb^{2+}-staining solution of CuPOH-Nafion.

3. References

1 J. Han, L. Bai, S. Luo, B. Yang, Y. Bai, S. Zeng and X. Zhang, *Sep. Purif. Technol.,* 2020, **248**, 117041.

2 B. P. Bandgar and P. B. Gujarathi, *J. Chem. Sci.,* 2008, **120**, 259-266

3 B. B. Beyene, A. M. Mihirteu, M. T. Ayana and A. W. Yibeltal, *Results in Chemistry,* 2020, **2**, 100073

4 T. Mabuchi and T. Tokumasu, *J. Chem. Phys.,* 2014, **141**.

5 Q. He, D. C. Joy and D. J. Keffer, *J. Power Sources,* 2013, **241**, 634-646.

6 M. Levitt, M. Hirshberg, R. Sharon, K. E. Laidig and V. Daggett, *J Phys. Chem. B,* 1997, **101**, 5051-5061.

7 S. S. Jang, V. Molinero, T. Çağın and W. A. Goddard, *J Phys. Chem. B,* 2004, **108**, 3149-3157.

8 V. Zoete, M. A. Cuendet, A. Grosdidier and O. Michielin, *J. Comput. Chem.,* 2011, **32**, 2359-2368.

9 S. Plimpton, *J. Comput. Phys.*, 1995, 117 (1), 1-19.

10 G. Kresse and J. Furthmüller, *Phys. Rev. B,* 1996, **54**, 11169-11186.

11 J. P. Perdew, K. Burke and M. Ernzerhof, *Phys. Rev. Lett.,* 1996, **77**, 3865-3868.

12 J.-C. Dong, X.-G. Zhang, V. Briega-Martos, X. Jin, J. Yang, S. Chen, Z.-L. Yang, D.-Y. Wu, J. M. Feliu, C. T. Williams, Z.-Q. Tian and J.-F. Li, *Nat. Energy,* 2019, **4**, 60-67.